



Quaternary ecological responses and impacts of the Indian Ocean Summer Monsoon at Nam Co, Southern Tibetan Plateau



Franziska Günther^a, Roman Witt^a, Stefan Schouten^{b,c}, Roland Mäusbacher^d,
Gerhard Daut^d, Liping Zhu^e, Baiqing Xu^e, Tandong Yao^e, Gerd Gleixner^{a,*}

^a Max Planck Institute for Biogeochemistry, Jena, Germany

^b NIOZ Royal Netherlands Institute for Sea Research, Department of Marine Organic Biogeochemistry, Den Burg, Texel, The Netherlands

^c Faculty of Geosciences, University of Utrecht, Utrecht, The Netherlands

^d Friedrich Schiller University, Jena, Germany

^e Key Laboratory of Tibetan Environment Changes and Land Surface Processes Institute of Tibetan Plateau Research, Chinese Academy of Sciences, Beijing, China

ARTICLE INFO

Article history:

Received 3 April 2014

Received in revised form

23 January 2015

Accepted 27 January 2015

Available online 14 February 2015

Keywords:

n-Alkanes

GDGTs

Hydrogen isotopes (δD)

$\delta^{15}N$

$\delta^{13}C_{org}$

Indian Ocean Summer Monsoon (IOSM)

Temperature

Precipitation

Time lag

Ecological thresholds

ABSTRACT

The transition from the Last Glacial to the current Interglacial, the Holocene, represents an important period with climatic and environmental changes impacting ecosystems. In this study, we examined the interplay between the Indian Ocean Summer Monsoon (IOSM) and the Westerlies at lake Nam Co, southern Tibet to understand the climatic effects on the ecosystem. Different organic geochemical proxies (*n*-alkanes, glycerol dialkyl glycerol tetraethers, δD , $\delta^{13}C_{org}$, $\delta^{15}N$) are applied to reconstruct the environmental and hydrological changes on one of the longest available paleorecords at the Tibetan Plateau. Based on our paleohydrological δD proxies, the aquatic signal lags the terrestrial one due to specific ecological thresholds, which, in addition to climatic changes, can influence aquatic organisms. The aquatic organisms' response strongly depends on temperature and associated lake size, as well as pH and nutrient availability. Because the terrestrial vegetation reacts faster and more sensitively to changes in the monsoonal and climatic system, the δD of *n*-C₂₉ and the reconstructed inflow water signal represent an appropriate IOSM proxy. In general, the interplay of the different air masses seems to be primarily controlled by solar insolation. In the Holocene, the high insolation generates a large land-ocean pressure gradient associated with strong monsoonal winds and the strongest IOSM. In the Last Glacial period, however, the weak insolation promoted the Westerlies, thereby increasing their influence at the Tibetan Plateau. Our results help to elucidate the variable IOSM, and they illustrate a remarkable shift in the lake system regarding pH, $\delta^{13}C_{org}$ and $\delta^{15}N$ from the Last Glacial to the Holocene interglacial period.

© 2015 Elsevier Ltd. All rights reserved.

1. Introduction

The Asian monsoon is an important component of the modern climate system, and it interacts with other subsystems, such as the El Niño–Southern Oscillation (ENSO) and the North Atlantic Oscillation (NAO) (Gupta et al., 2003; Kumar et al., 2006). The main driver of the Asian monsoon is the thermally induced pressure gradient between land and ocean based on their different warming (Li and Yanai, 1996). Therefore, the Tibetan Plateau may act as an elevated heat source that can enhance the Asian monsoon (An et al.,

2001; Wu et al., 2012). This area is mainly influenced by the Indian Ocean Summer Monsoon (IOSM), which delivers the majority of the precipitation in the summer months, and by the Westerlies in the winter months (Leber et al., 1995; IAEA/WMO, 2012). However, the extent of the IOSM has changed, and several proxies have been used to track the variability of monsoon winds and/or monsoonal precipitation in the past (cf. Wang et al., 2005; Morrill et al., 2003, 2006). Oxygen isotope records from caves and ice cores are usually used to record the precipitation and temperature signal, respectively (Thompson et al., 1997; Grootes et al., 1999; Petit et al., 1999; Sinha et al., 2005; Shakun et al., 2007). The planktonic foraminifera *Globigerina bulloides* are often applied to track monsoon winds (Overpeck et al., 1996; Kudrass et al., 2001; Gupta et al., 2003).

* Corresponding author. Tel.: +49 3641 576172; fax: +49 3641 5770.

E-mail address: gerd.gleixner@bgc-jena.mpg.de (G. Gleixner).

Over the last decade, hydrogen isotopes (δD) of *n*-alkanes have increasingly been used as a paleohydrological proxy (cf. Sachse et al., 2012 and references therein). *n*-Alkanes can be attributed to either aquatic or terrestrial organisms and reflect, among other factors, the isotope signal of their source water in their δD signal. Aquatic *n*-alkanes, which in Tibetan lakes predominantly comprise less than 25 carbon atoms, mainly record the isotope signal of the lake water (Günther et al., 2013). In contrast, terrestrial *n*-alkanes, which predominantly comprise more than 27 carbon atoms in Tibetan ecosystems, mainly reflect the meteoric water (Günther et al., 2013). The isotope signal is modified by evaporation as well as by transpiration and biosynthetic fractionation (Sessions et al., 1999; Mügler et al., 2008). Lacustrine *n*-alkanes are persistent over geological timescales and, therefore, enable the reconstruction of both lake water and meteoric water in paleoclimate studies (Schimmelmann et al., 1999; Pedentchouk et al., 2006). Glycerol dialkyl glycerol tetraethers (GDGTs) are membrane lipids that are often applied to reconstruct air and water temperatures in lacustrine systems (e.g., Sinninghe Damsté et al., 2009; Blaga et al., 2010; Wang et al., 2012). Branched GDGTs (bGDGTs) are mainly produced by bacteria, and their degree of cyclization (CBT) is correlated with soil pH (Weijers et al., 2007) as well as lake water pH (Schoon et al., 2013; Günther et al., 2014). The methylation of bGDGTs is correlated with air temperature and (soil/water) pH (Peterse et al., 2012; Günther et al., 2014). Isoprenoid GDGTs (iGDGTs) of archaeal origin are used to estimate water temperatures based on the TEX₈₆ proxy (Schouten et al., 2002; Günther et al., 2014). Moreover, bulk organic isotope records ($\delta^{13}C_{org}$, $\delta^{15}N$) are used to describe the state and development of the lake system. $\delta^{13}C_{org}$ is a proxy used to determine the contribution of aquatic and terrestrial organic matter sources (Meyers, 1994), and $\delta^{15}N$ serves as a proxy for autochthonous primary production and the nutrient availability in lakes (Kendall, 1998).

These proxies are used to reconstruct the IOSM's dynamics and its impact on lacustrine sediments of lake Nam Co, on the southern part of the Tibetan Plateau. Numerous lake studies at the Tibetan Plateau have focused on changes of the IOSM during the Holocene (e.g., Morrill et al., 2006; Mügler et al., 2010; Kasper et al., 2012; Doberschütz et al., 2013), but only a few have investigated the transition from the Pleistocene to the Holocene (partially in Morrill et al., 2003; Liu et al., 2007; Wünnemann et al., 2010; Yan and Wünnemann, 2014). The current investigation focuses on the transition from the Last Glacial Maximum (LGM) to the Early Holocene and is an extension of the already-published Nam Co data covering the Holocene (Mügler et al., 2010). We analyzed the interplay between the IOSM and Westerlies as well as the related climatological, ecological and hydrological changes, at Nam Co during this period.

2. Materials and methods

2.1. Study site

With a water area of approximately 1920 km², Nam Co (30°30'–30°56' N; 90°16'–91°03' E; 4722 m a.s.l.) is the second-largest saline lake on the Qinghai–Tibetan Plateau (Fig. 1). The total catchment area spans 10,610 km² (Guan et al., 1984). The mean relative humidity is 52.6% (for 2005–2006) (Li et al., 2007). The mean annual air temperature (MAAT) is 0 °C, with a minimum of –26.4 °C (in February 2005–2006) and a maximum of 20.6 °C (in July 2005–2006) (Keil et al., 2010). The mean annual precipitation is approximately 281 mm, with the majority of precipitation between June and October delivered by the IOSM (Hren et al., 2009). From January to May, Westerly winds influence the lake (Keil et al., 2010). Precipitation and rivers, primarily entering the lake in the southern

part, are the most important water supplies. Rivers are recharged by precipitation and glacial melt water from the adjacent Nyainqen-tanglha Mountain. Nam Co has no outflow, and hence, its water balance is solely controlled by the water input and evaporation. The mean annual evaporation from the lake surface and catchment is 790 mm and 320 mm, respectively (Zhu and Meng, 2004). Evaporation exceeds precipitation, and Nam Co is characterized by a semi-arid climate (Feng et al., 2006). The maximum water depth is approximately 99 m (Daut et al., 2010). The lake water is characterized by a high pH (from 8 to 9.7, averaging at 9.21) and a salinity of 1.8 g/l (in the years 2006–2008) (Wang et al., 2009).

2.2. Sampling and sample preparation

The sediment core NC 08/01 (30° 44' 14.71" N; 90° 47' 25.19" E), with a total length of approximately 10.4 m, was recovered from a water depth of approximately 93 m using a piston corer (UWITEC, Mondsee, Austria). Opening and sampling of the core was carried out at the geoecological–sedimentological laboratory at the University of Jena, Germany. The sediment samples were freeze-dried and homogenized for further analysis.

2.3. Dating

In total, 24 bulk samples of the sediment core were used for AMS ¹⁴C radiocarbon dating carried out at Beta Analytics, Miami, USA. Based on the dating of recent sediments, the reservoir effect accounts for 1420 years (Kasper et al., 2012; Doberschütz et al., 2013). The modern ¹⁴C reservoir age correction was applied for the entire core NC 08/01. The sediment core was sampled in 1-cm slices at 5-cm intervals and, according to the sedimentation rate, was pooled for lipid biomarker analysis, resulting in a mean time resolution of approximately 100 years.

2.4. Analysis of lipid biomarker compounds

Depending on the organic carbon content, 2–9 g of sample was used for lipid extraction. Total lipids were extracted twice with a mixture of dichloromethane/methanol (9:1, v:v) at 100 °C and 138 bar for 15 min using an accelerated solvent extractor (ASE-200, DIONEX Corp., Sunnyvale, USA). Activated copper was added to remove elemental sulfur. Total lipid extracts were separated over an activated silica gel column into aliphatic, aromatic and polar fractions and were eluted with hexane, chloroform and methanol, respectively (Sachse et al., 2006).

2.4.1. GDGTs

Glycerol dialkyl glycerol tetraethers (GDGTs) were analyzed at the Royal Netherlands Institute for Sea Research (NIOZ), Texel, Netherlands. Aliquots of the polar fractions were added with a known amount of an internal C₄₆ GDGT standard (Huguet et al., 2006), dried under N₂, re-dissolved in hexane/isopropanol (99:1, v:v) and filtered through a PTFE syringe filter (0.45-μm pore size, 4-mm diameter). Ten milliliters of each sample was measured using high-performance liquid chromatography/atmospheric pressure positive ion chemical ionization-mass spectrometry (HPLC/APCI-MS) on an Agilent (Palo Alto, CA) 1100 LC/MSD SL system according to Schouten et al. (2007). The [M+H]⁺ ions of the individual GDGTs were measured with single ion monitoring (SIM). Peak areas were integrated following the method of Weijers et al. (2007). The cyclization (CBT) of branched tetraether was calculated to compute pH using equations (1)–(2) with eq. (2) representing the local calibration for lakes on the Tibetan Plateau (Günther et al., 2014). The simplified methylation (MBT') of branched tetraethers was used to determine the mean air temperature (MAT) using equations

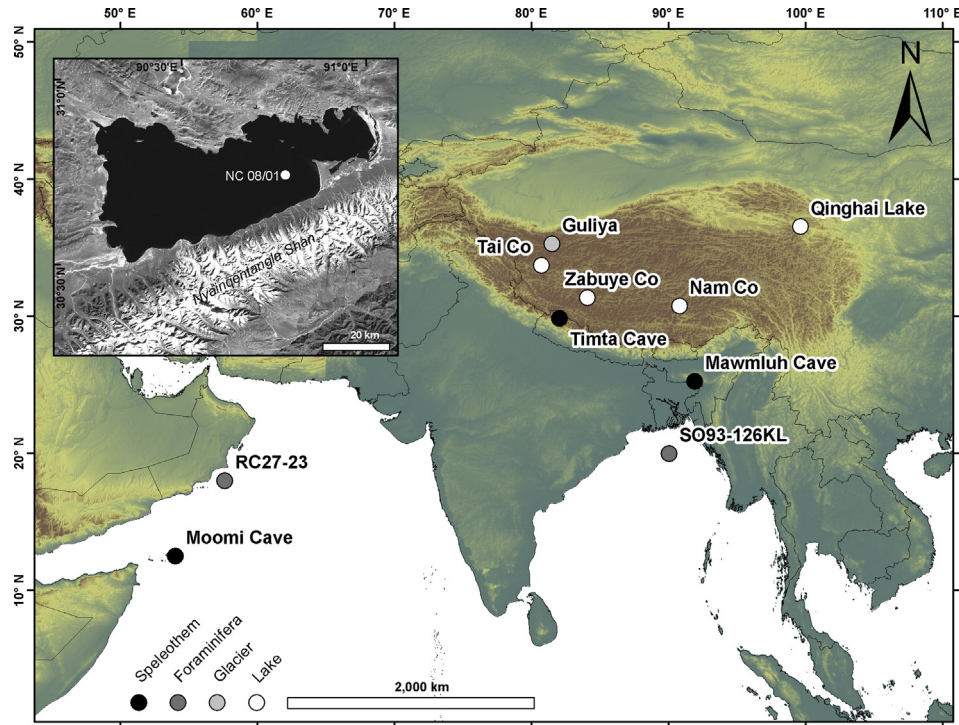


Fig. 1. Nam Co and other study sites mentioned in the text: speleothems (Sinha et al., 2005; Shakun et al., 2007; Berkelhammer et al., 2012), foraminifera (Overpeck et al., 1996; Kudrass et al., 2001) and glacier (Thompson et al., 1997). Inset map shows the location of sediment core NC 08/01 in Nam Co.

(3)–(4). Based on iGDGTs, TEX_{86} as a proxy for water temperature can be calculated (equations (5)–(6)). GDGT numbers refer to structures in Schouten et al. (2013).

$$\text{CBT} = -\log\left(\frac{\text{bGDGT Ia} + \text{bGDGT IIa}}{\text{bGDGT I} + \text{bGDGT II}}\right) \quad (\text{after Weijers et al., 2007}) \quad (1)$$

$$\text{pH} = 7.97 + 2.78 \times \text{CBT} \quad (\text{after Günther et al., 2014}) \quad (2)$$

of the aliphatic fraction were separated on a DB1ms column (30 m, 0.25-mm ID, 0.25- μm film thickness; Agilent Technologies, Santa Clara, USA) at a constant helium carrier gas flow of 2 ml/min. The PTV injector operated in splitless mode at an initial temperature of 45 °C and was heated up to 300 °C. The GC oven program increased from 90 °C (held for 1 min) to 300 °C (held for 9 min) with 10 °C/min and finally to 335 °C (held for 3 min) with 30 °C/min.

$$\text{MBT}' = \frac{\text{bGDGT I} + \text{bGDGT Ia} + \text{bGDGT Ib}}{\text{bGDGT I} + \text{bGDGT Ia} + \text{bGDGT Ib} + \text{bGDGT II} + \text{bGDGT IIa} + \text{bGDGT IIb} + \text{bGDGT III}} \quad (\text{after Peterse et al., 2012}) \quad (3)$$

$$\text{MAT} = 0.81 - 5.67 \times \text{CBT} + 31.0 \times \text{MBT}' \quad (\text{after Peterse et al., 2012}) \quad (4)$$

$$\text{TEX}_{86} = \frac{\text{iGDGT2} + \text{iGDGT3} + \text{iGDGT IV}'}{\text{iGDGT 1} + \text{iGDGT2} + \text{iGDGT 3} + \text{iGDGT IV}'} \quad (\text{after Schouten et al., 2002}) \quad (5)$$

$$\text{LST} = 54.89 \times \text{TEX}_{86} - 13.36 \quad (\text{after Castañeda and Schouten, 2011}) \quad (6)$$

2.4.2. *n*-Alkanes

The aliphatic fraction in hexane was injected (1 μl) into a gas chromatograph with flame ionization detection (TRACE-GC 2000; CE Instruments, Thermo Quest, Rodano, Italy) for quantification of *n*-alkanes. Identification was performed by comparison to an external *n*-alkane standard mixture (*n*-C₁₅ to *n*-C₃₁). Compounds

2.5. Isotope analysis

2.5.1. Organic carbon and nitrogen stable isotope analyses ($\delta^{13}\text{C}_{\text{org}}$, $\delta^{15}\text{N}$)

For $\delta^{13}\text{C}_{\text{org}}$ analysis, 1–5 mg of the sample was weighed into tin capsules depending on the carbon content. Inorganic carbon was removed by the gradual addition of 120 μl sulfurous acid (Steinbeiss et al., 2008). For $\delta^{15}\text{N}$ analysis, 40–80 mg of the sample was

weighed into tin capsules depending on the nitrogen content. All capsules were introduced into an NA 1110 CN elemental analyzer (CE Instruments, Rodano, Italy). The produced gases were transferred to an isotope-ratio mass spectrometer (Delta C, equipped with a Delta⁺ ion source; Finnigan MAT, Bremen, Germany) via a ConFlo III interface (FinniganMAT) for isotope measurement (Werner et al., 1999). Each sample was measured at least twice. The standard deviation was approximately 0.07‰ for $\delta^{13}\text{C}_{\text{org}}$ and $\delta^{15}\text{N}$.

2.5.2. Hydrogen isotope analysis of *n*-alkanes

Compound-specific hydrogen isotopes were obtained using a coupled GC–IRMS system (GC: HP5890, Agilent Technologies, Palo Alto USA; IRMS: Delta⁺ XL, Thermo Fisher Scientific, Bremen, Germany) equipped with a DB1ms column (50 m, 0.32-mm ID, 0.52- μm film thickness; Agilent Technologies, Santa Clara, USA). The injector worked at 280 °C in splitless mode. The oven program started at 60 °C (held for 2 min) and heated up to 320 °C (held for 10 min) with 6 °C/min. Throughout the run, the column flow was held constant at 1.7 ml/min. To monitor possible co-elution with other components, 5% of the samples were forwarded to an ion trap mass spectrometer (GCQ ThermoElectron, San Jose, USA). Isotope ratios were normalized to the Vienna Standard Mean Ocean Water (V-SMOW) scale using a standard mixture of *n*-alkanes (*n*-C₁₅ to *n*-C₃₁). The standard mixture was measured after a maximum of three samples to verify the accuracy of the analysis. If necessary, a drift correction was applied to the δD values of the samples (Werner and Brand, 2001). The results are reported as conventional delta notation in per mil relative to V-SMOW (‰ vs. V-SMOW). Each sample was measured at least three times, and the standard deviation of replicate measurements for all peaks was 4.8‰ in the standard mixture. The H_3 factor, which confirms stable ion source conditions, was determined once a day with pulses of increasing reference gas amount and had a standard deviation of 0.50.

Despite volume reduction to 20 μl before injection, many sediment samples still contained low amounts of *n*-alkanes. Therefore, only peaks with amplitudes over 50 mV were directly used for evaluation. Peaks smaller than 50 mV have to be size corrected according to Polissar et al. (2009). To calculate the δD values, ISO-DAT NT 2.0 (Thermo Fisher Scientific, Bremen, Germany) was used to apply individual background correction. Outliers in the δD values were identified according to Grubbs (1969) and excluded from further calculations.

2.6. δD correction for the global ice volume effect

The δD of terrestrial *n*-alkanes was corrected due to the more enriched ocean and precipitation values during glacial periods. Since the LGM, the global ice volume effect accounts for 8‰ (Schrager et al., 1996). The correction for δD values was calculated after Wang et al. (2013):

$$\delta\text{D} = \delta\text{D}_{\text{measured}} - 8 \times \delta^{18}\text{O}_{\text{ice-volume}} \times \left(1 + \frac{\delta\text{D}_{\text{measured}}}{1000}\right) / \left(1 + 8 \times \frac{\delta^{18}\text{O}_{\text{ice-volume}}}{1000}\right) \quad (7)$$

We used simulated marine oxygen isotopes to reconstruct changes in the past ice volume (Bintanja et al., 2005). The $\delta^{18}\text{O}$ record was interpolated to match the sediment sample ages.

2.7. Calculation of δD values for lake and inflow waters

Based on significant correlations between δD of *n*-C₂₃ with δD of lake water and δD of *n*-C₂₉ with δD of inflow water, calibration

functions for the Tibetan Plateau were established to convert the δD of sedimentary *n*-alkanes to the primary lake ($\delta\text{D}_{\text{LW}}$) and inflow ($\delta\text{D}_{\text{IW}}$) water isotope composition (Günther et al., 2013):

$$\delta\text{D}_{\text{LW}} = (\delta\text{D}_{\text{C23}} + 46.34)/1.89 \quad (R^2 = 0.94, p < 0.001) \quad (8)$$

$$\delta\text{D}_{\text{IW}} = (\delta\text{D}_{\text{C29}} + 129.18)/0.70 \quad (R^2 = 0.66, p = 0.003) \quad (9)$$

2.8. Calculation of the lake water balance

The lake water balance in the form of the remaining water fraction (*f*) can be modeled by the Rayleigh distillation, which describes the progressive deuterium enrichment of an evaporating water body:

$$R = R_0 \cdot f^{(\alpha - 1)} \quad (10)$$

with R_0 as the hydrogen isotope ratio of the precipitation as the initial isotope signal, *R* as the isotope ratio of the remaining lake water and α as fractionation factor. Detailed information on the Rayleigh process and function are given in Clark and Fritz (1997).

3. Results

The results from our long core NC 08/01 extend the already-published dataset from sediment core NC 8, which dates back to 7.3 cal ka BP (Mügler et al., 2010). We will therefore focus on the time period from 23.7 to 7.5 cal ka BP in the following discussion.

3.1. Chronology

Based on the reservoir-corrected AMS ¹⁴C-ages, the sediment core dates back to 23.7 cal ka BP, and the sediment accumulation rates vary between 2.4 and 0.1 mm/a (Kasper et al., 2015). The chronology and lithology of the sediment core was already described in detail by Kasper et al. (2015). We used a constant reservoir correction, while noting that reservoir effects may have varied in the past (Geyh et al., 1998). The chronology in the upper part of this composite core was evaluated by paleomagnetic measurements and their agreement with geomagnetic field models (Kasper et al., 2012).

3.2. Distribution and concentration of biomarkers

The total *n*-alkane amounts range from 270 to 4750 ng/g dry weight, with the highest amounts in the Holocene. The *n*-alkane records show a clear increase after 12 cal ka BP (Fig. 2). C₂₃ is the most abundant *n*-alkane in the sediments, with up to 980 ng/g dry weight. In general, aquatic *n*-alkanes (C₂₃) are more abundant than terrestrial *n*-alkanes (C₂₉) (ratio C₂₃:C₂₉ = 1.4:1).

Low amounts of crenarchaeol, bGDGTs and iGDGTs are measured for the period from 23.7 to 15 cal ka BP with 12 ± 14 , 93 ± 42 and 24 ± 16 ng/g dry weight, respectively (Fig. 2). After 15 cal ka BP, concentrations of crenarchaeol, bGDGTs and iGDGTs increase up to 810, 2630 and 1490 ng/g dry weight, respectively. The CBT values change from 0.47 ± 0.11 (23.7–16.7 cal ka BP) to 0.12 ± 0.11 (16.7–7 cal ka BP). The reconstructed pH also shows a decrease of 1 pH unit (from 9.3 ± 0.3 to 8.3 ± 0.3) in the mentioned periods (Fig. 3). In contrast, the TEX₈₆ values do not significantly change and remain quite constant for the whole record, at 0.35 ± 0.05 . The reconstructed LST and SLST, based on TEX₈₆, is 5.8 ± 2.5 and 10.6 ± 2.1 °C, respectively (Fig. 3).

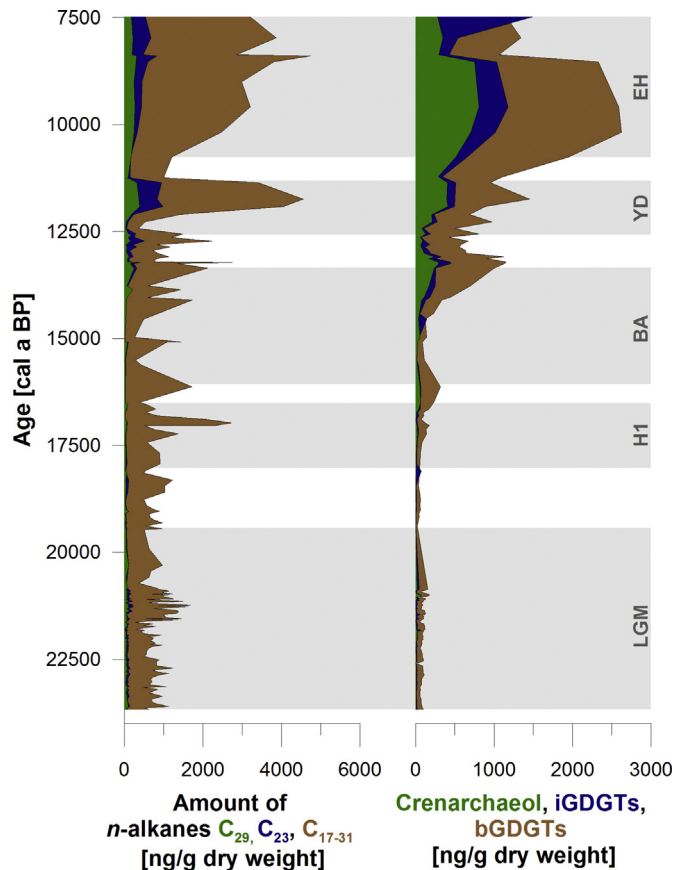


Fig. 2. Total amounts of *n*-alkanes (C_{29} , C_{23} , C_{17-31}) and GDGTs (crenarchaeol, iGDGTs, bGDGTs) in the sediment core from Nam Co.

3.3. Isotopic characteristics

3.3.1. Bulk isotopes ($\delta^{13}C_{org}$, $\delta^{15}N$)

The sediment core can be divided into two sections by means of $\delta^{13}C_{org}$ and $\delta^{15}N$. From 23.7 to 15.5 cal ka BP, the $\delta^{13}C_{org}$ values are heavier with values of $-22.7 \pm 1.1\text{‰}$. In the last 15.5 cal ka BP, $\delta^{13}C_{org}$ values are lower, at $-24.4 \pm 0.6\text{‰}$ (Fig. 3). From 23.7 to 14 cal ka BP, the $\delta^{15}N$ values are continuously depleted and remain quite stable during the Holocene. The period from 23.7 to 14 cal ka BP is characterized by a $\delta^{15}N$ of $7.6 \pm 0.8\text{‰}$, while in the last 14 cal ka BP, the $\delta^{15}N$ values are $5.0 \pm 0.3\text{‰}$ (Fig. 3).

3.3.2. Compound-specific hydrogen isotopes

We focus on the *n*-alkanes C_{23} and C_{29} as aquatic and terrestrial biomarkers, which reflect the isotope signal of the lake and inflow water, respectively (Günther et al., 2013). In general, the δD values of *n*- C_{23} vary between -61 and -233‰ . Based on the mean δD values for the different climate periods, the lowest values are recorded during the Early Holocene (10.8–7 cal ka BP), at $-186 \pm 31\text{‰}$, and the strongest enrichment is measured during the Bølling–Allerød (16.8–13.8 cal ka BP), at $-95 \pm 38\text{‰}$ (Fig. 3). The deduced lake water δD values (after equation (8)) range from -8 to -99‰ , showing the same pattern for mean δD values with the highest depletion during the Early Holocene ($-74 \pm 17\text{‰}$) and the highest enrichment ($-26 \pm 20\text{‰}$) during the Bølling–Allerød (Fig. 3).

The δD values of *n*- C_{29} vary between -136 and -280‰ . After correction for the global ice volume effect, the δD values of *n*- C_{29} are between -148 and -284‰ . The amendment resulted in a shift

of $-7.3 \pm 3.8\text{‰}$ in the glacial period, without changing the overall pattern (Fig. 3). Converting the corrected δD of *n*- C_{29} into inflow water δD (after equation (9)) results in values from -27 to -249‰ . Comparable to the δD of *n*- C_{23} , the strongest depletion for the mean δD values is recorded for the period of the Early Holocene ($-203 \pm 12\text{‰}$), but the highest enrichment is measured in the glacial periods, during the LGM and Heinrich 1, at $-106 \pm 33\text{‰}$ (Fig. 3). Based on the evaporation model (Appendix A1), the highest evaporation is recorded during the Bølling–Allerød (evaporation to inflow, E/I ratio of 10.7 ± 3.5). Less evaporation with inflow exceeding evaporation is recorded for the glacial periods LGM and Heinrich 1 (E/I ratio of 0.26 ± 0.77) (Fig. 3).

4. Discussion

4.1. Does the paleohydrological δD proxy display the IOSM?

We compared the δD of *n*- C_{29} with distinctive proxies from the source area of the IOSM to validate the monsoon influence on our paleohydrological proxy from Nam Co (Fig. 1). In general, two aspects of the monsoon can be reconstructed: either monsoon winds or monsoon-induced precipitation (Wang et al., 2005). Carbonate oxygen isotopes ($\delta^{18}O_{carb}$) are commonly used to reconstruct the monsoon intensity in terms of precipitation (Sinha et al., 2005; Shakun et al., 2007), while foraminifera such as *Globigerina bulloides* ($\delta^{18}O_{G.bulloides}$) reflect monsoon-induced upwelling, which is controlled by monsoon winds (Overpeck et al., 1996; Kudrass et al., 2001).

All records, $\delta^{18}O_{carb}$ as well as $\delta^{18}O_{G.bulloides}$, showed an initial increase in the IOSM associated with depleted oxygen isotopes during the Bølling–Allerød and a second change in the Early Holocene (Appendix A2). Our δD values of *n*- C_{29} , which reflect the precipitation signal modified by evapotranspiration, are in best agreement with the Bay of Bengal $\delta^{18}O_{G.bulloides}$ record (Kudrass et al., 2001). This can be attributed to the most important trajectory in which the moisture is transported from the Bay of Bengal over the Brahmaputra river valley to the Nam Co (Tian et al., 2001). Variations in the exact timing of IOSM changes are caused by site-specific differences such as local topography or regional river water input as well as by inaccuracies in the age models. The δD and $\delta^{18}O$ records showed a similar pattern, and thus, our paleohydrological proxies do reflect the IOSM signal at Nam Co. In the LGM, the $\delta^{18}O$ records are highly enriched and do not exhibit large variations, pointing to a continuously weak IOSM. Changes in the δD of *n*- C_{29} in this period may be caused by other factors, such as lower temperatures or the increasing participation of isotopically light sublimated snow from the Western Tibetan Plateau that is transported to Nam Co by enhanced Westerlies.

4.2. Variability of IOSM and its influence on the Nam Co

Changes in the precipitation as well as temperature can be used to better understand the monsoon system in the past. At present, temperature and precipitation are positively correlated with each other because both show the highest values during the summer months, which are affected by the IOSM (Lhasa; IAEA/WMO, 2012). However, the amount effect has the largest impact on the isotopic composition of precipitation at Nam Co (Hren et al., 2009).

Based on the precipitation and temperature records of lake Nam Co, the LGM (23.7–19.4 cal ka BP) on the southern Tibetan Plateau is characterized by a weak IOSM. Precipitation amounts were lower (enriched δD *n*- C_{29}) than the present (Fig. 3). The more depleted values of *n*- C_{29} at 21.7 cal ka BP may be attributed to lower temperatures or the increased influence of Westerly air masses transporting isotopically depleted sublimated snow from Central Asia to

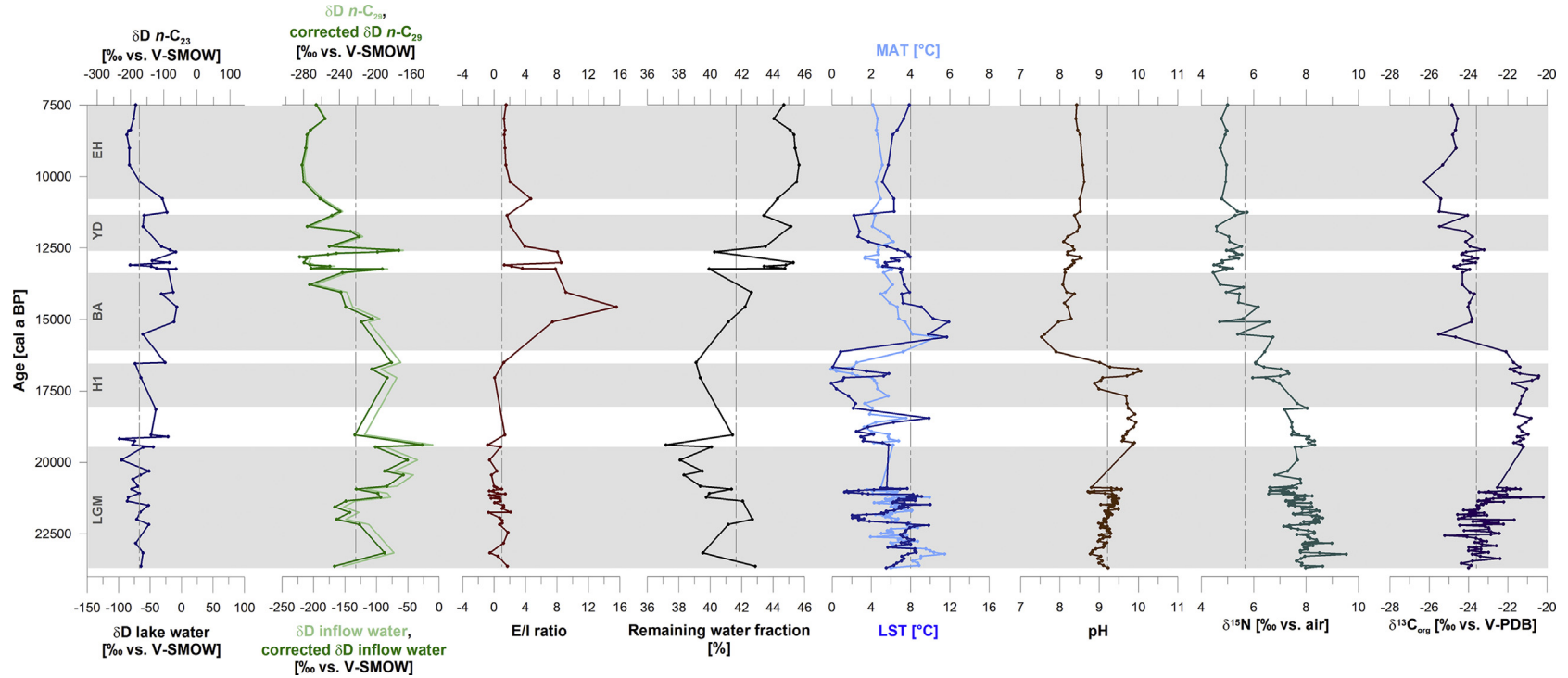


Fig. 3. Hydrogen isotope values (δD) of $n\text{-C}_{23}$ and $n\text{-C}_{29}$, reconstructed δD of lake and inflow water, δD of $n\text{-C}_{29}$ and inflow water corrected for ice volume effect, evaporation-to-inflow (E/I) ratio, remaining water fraction in the lake, lake surface temperature (LST), as well as the mean air temperature (MAT), pH values, $\delta^{15}\text{N}$ and $\delta^{13}\text{C}_{\text{org}}$ values for Nam Co sediments. A 3-point smoothing was performed for hydrogen isotope records to set the secular trend. The broken light gray lines indicate the present values. Gray bars represent important climate periods (LGM – Last Glacial Maximum, H1 – Heinrich 1, BA – Bølling–Allerød, YD – Younger Dryas, EH – Early Holocene).

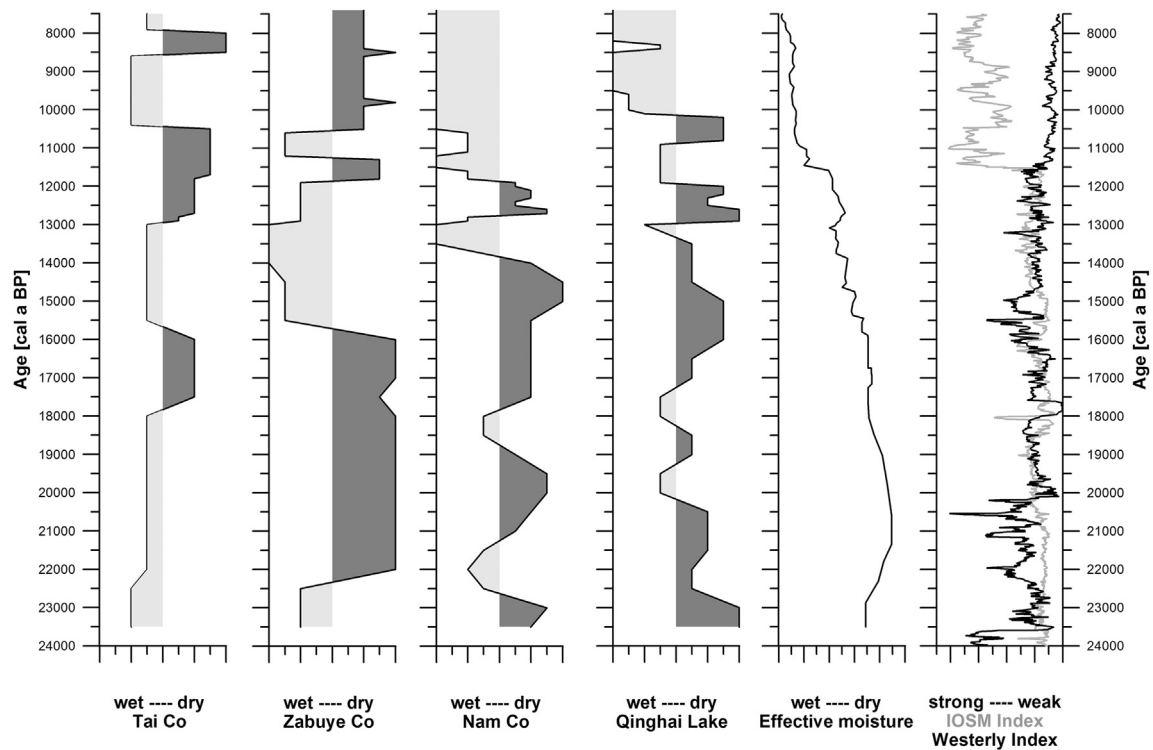


Fig. 4. Wet and dry periods in Tibetan lake systems Tai Co (Zheng et al., 2011), Zabuye Co (Wang et al., 2002), Nam Co (this study) and Qinghai Lake (Ji et al., 2005; An et al., 2012) based on a five-class ordinal index compared to the effective moisture (Herzschuh, 2006) and intensity indices of IOSM and Westerlies (An et al., 2012). Lake systems are presented in west–east direction.

the Eastern Tibetan Plateau. The Guliya ice core record in the western part of the Tibetan Plateau (Fig. 1) also showed lower oxygen isotope values in the Last Glacial than in the Holocene interglacial due to the stronger impact of temperature on ice core $\delta^{18}\text{O}$ values and the decreased temperatures (Thompson et al., 1997). The extension of the Westerlies across the Plateau in the glacial period is even more obvious when comparing different lake records. We compiled four different lake systems and differentiated their hydrological characteristics (based on sedimentological, geochemical or biological indicators and stable isotope records) into eight categories, from exceptionally dry to very wet conditions (Fig. 4). Dry periods are characterized by decreasing lake levels and wet periods by increasing lake levels. Tai Co in western Tibet, for example, was characterized by prolonged wet conditions, whereas lakes in the eastern part were less affected by this moisture (Fig. 4). Based on different climate indices, stronger Westerlies and a weaker IOSM were also observed at Qinghai Lake (Fig. 4). However, the low effective moisture at Nam Co (remaining water fraction in Fig. 3) and in Asia (Fig. 4) indicates that during the Glacial, the Westerlies transported less moisture than the current IOSM. The calculated mean annual lake surface temperature (LST) in the LGM was 1.8°C colder than the present (Fig. 3). This value is in agreement, considering the calibration error of the TEX_{86} proxy, with the modeled surface temperature decrease of approximately $2\text{--}4^\circ\text{C}$ compared to present values for East Asia (Ju et al., 2007). However, the temperature reconstructions at Nam Co should be considered tendencies rather than absolute values due to the various factors influencing lake water temperatures, such as lake depth and volume, ice thickness or melt water input. Due to the lower temperatures, the E/I ratio showed low values, indicating more humid conditions. Comparative conditions were also recorded in the Heinrich 1 ($18.1\text{--}16.5$ cal ka BP) and Younger Dryas ($12.6\text{--}11.4$ cal ka BP) (Fig. 3). In these cold periods, the monsoon

intensity decreased, while in warm periods, a strengthening of the IOSM is measured. We detected the onset of the IOSM associated with increased precipitation (depleted $\delta\text{D } n\text{-C}_{29}$) and temperature during the Bølling–Allerød ($16.1\text{--}13.8$ cal ka BP) (Fig. 3). In this period, the highest temperatures were recorded for the Pleistocene and are similar to present-day values. The highly enriched $\delta\text{D } n\text{-C}_{23}$ values are caused by strong evaporation, which is also confirmed by the E/I ratio. The strongest IOSM with persistently high amounts of precipitation (depleted $\delta\text{D } n\text{-C}_{29}$, depleted $\delta\text{D } n\text{-C}_{23}$) and increasing temperatures was recorded in the Early Holocene ($10.8\text{--}7$ cal ka BP) (Fig. 3). The spatio-temporal comparison of different records shows the decreasing influence of the IOSM towards the western part of the Plateau in the Early Holocene. Nam Co and Qinghai Lake as well as surrounding areas (e.g. Yan and Wünnemann, 2014), showing a similar moisture evolution, seem to be influenced by this moisture source (Fig. 4). The lake level rise in the Early Holocene is caused by both strong monsoonal precipitation (depleted $\delta\text{D } n\text{-C}_{29}$) and increased melt water input (depleted $\delta\text{D } n\text{-C}_{23}$) from the adjacent glaciers due to rising temperatures. The evaporation-to-inflow ratio is continuously decreasing, and most of the moisture is stored in the lake (remaining water fraction), resulting in the highest lake level stands for the investigated period.

Changes in the IOSM as well as in the climate conditions have a great influence on the lake system. The environmental conditions in the Early Holocene, for example, favored the bioproductivity that is reflected in the total amount of *n*-alkanes and GDGTs (crenarchaeol, iGDGTs, bGDGTs) (Fig. 2). Higher total abundances may also be the result of anoxic conditions and the hampered degradation of organic matter at the lake bottom. The reduced oxygen availability at the lake bottom usually occurs during high lake level stands and lake water stratification that can be connected to an increase in precipitation and temperature. Hence, the higher

amounts of *n*-alkanes and GDGTs are presumably the result of enhanced bioproductivity and better preservation in the lake system (Fig. 2). An initial slight increase in the bioproductivity and preservation was already detected in the Bølling–Ållerød, which is also characterized by higher temperatures and an increase in precipitation. The first warming in the final stage of the Last Glacial period, the Bølling–Ållerød, was an important period when the lake system showed an obvious change in pH and $\delta^{13}\text{C}_{\text{org}}$ values (Fig. 3). Before the Bølling–Ållerød, the $\delta^{13}\text{C}_{\text{org}}$ values continuously increased (up to -20.4‰), while after 13.8 cal ka BP, there was a tendency toward more depleted values ($-24.4 \pm 0.6\text{‰}$) (Fig. 3). In general, our $\delta^{13}\text{C}_{\text{org}}$ values correspond to plants using the C3 pathway (Meyers, 1994; Meyers and Ishiwatari, 1995). In addition to the different carbon fixation pathway, the available dissolved CO_2 as a carbon source and the amount of primary production, combined with the release of light CO_2 during organic matter decomposition, can influence the $\delta^{13}\text{C}_{\text{org}}$ values (Hayes, 1993; Laws et al., 1995). In the glacial, lower CO_2 concentrations led to decreasing fractionation, and the storage of old ^{13}C -depleted carbon in the oceans involved enriched $\delta^{13}\text{C}$ in the atmosphere (Schmitt et al., 2012).

Because dissolved CO_2 from the respiration of decomposing aquatic plants and phytoplankton in the lake system led to depleted $\delta^{13}\text{C}$ values, we could detect an increase in bioactivity at the beginning of the Bølling–Ållerød. This period was also characterized by changes in the atmospheric CO_2 (Fig. 5). Due to the release of old carbon from the deep ocean, CO_2 increased and $\delta^{13}\text{C}$ decreased at 17.5 cal ka BP and reached their minima at 16 cal ka BP (Schmitt et al., 2012). These results are in agreement with our data and show the importance of atmospheric CO_2 as a carbon source. The two different isotopic stages in our $\delta^{13}\text{C}_{\text{org}}$ record mainly display different productivity levels controlled by environmental conditions. The transition between the different $\delta^{13}\text{C}_{\text{org}}$ stages points to ecological thresholds (see below) driving the system.

The same pattern is also observable in the pH values. Changes in pH can be attributed to melt water supply or increased precipitation, which currently has pH values of 6.6 (Li et al., 2007). The hydrochemistry of the lake water can be altered due to the mixing of the lake water with increased precipitation and inflow. Another explanation for the lower pH values is the increase in bio-productivity as a response to temperature changes and the enlarged input of organic carbon transported by precipitation. With higher respiration than photosynthesis rates, organic carbon is decomposed, and CO_2 is released in the lake water, lowering the pH and concurrently depleting the $\delta^{13}\text{C}_{\text{org}}$ values.

The $\delta^{15}\text{N}$ values also show a change from one stage into another, but the transition lasts longer than that for $\delta^{13}\text{C}_{\text{org}}$ and pH. In the LGM, $\delta^{15}\text{N}$ was invariable (7.8 ± 0.5) as well as in the period after the Bølling–Ållerød (5.0 ± 0.3) (Fig. 3). The change to more depleted values can be ascribed to a more abundant nitrogen supply or to an enhanced nitrogen fixation by legumes (Fry, 1991; Kendall, 1998). This is well known for regenerating ecosystems (Rothe and Gleixner, 2004). However, the complex interactions between the processes influencing the $\delta^{15}\text{N}$ values may explain the prolonged transition time.

4.3. Ecological thresholds for aquatic organisms at Nam Co

Climatically induced ecological thresholds are defined as critical values or periods where the biological response changes rapidly to small variations in the climate system (Huggett, 2005). In general, lakes can have different characteristics and, therefore, different climate sensitivity thresholds. Changes in effective moisture (precipitation–evaporation), for example, influence the lake levels and the associated salinity, which influences the aquatic organisms. In our records, the response of the aquatic system lags changes in the terrestrial signal by 5 ka in the Last Glacial period and by 1.2 ka in the Holocene (Fig. 6). Aquatic organisms seem to be influenced not

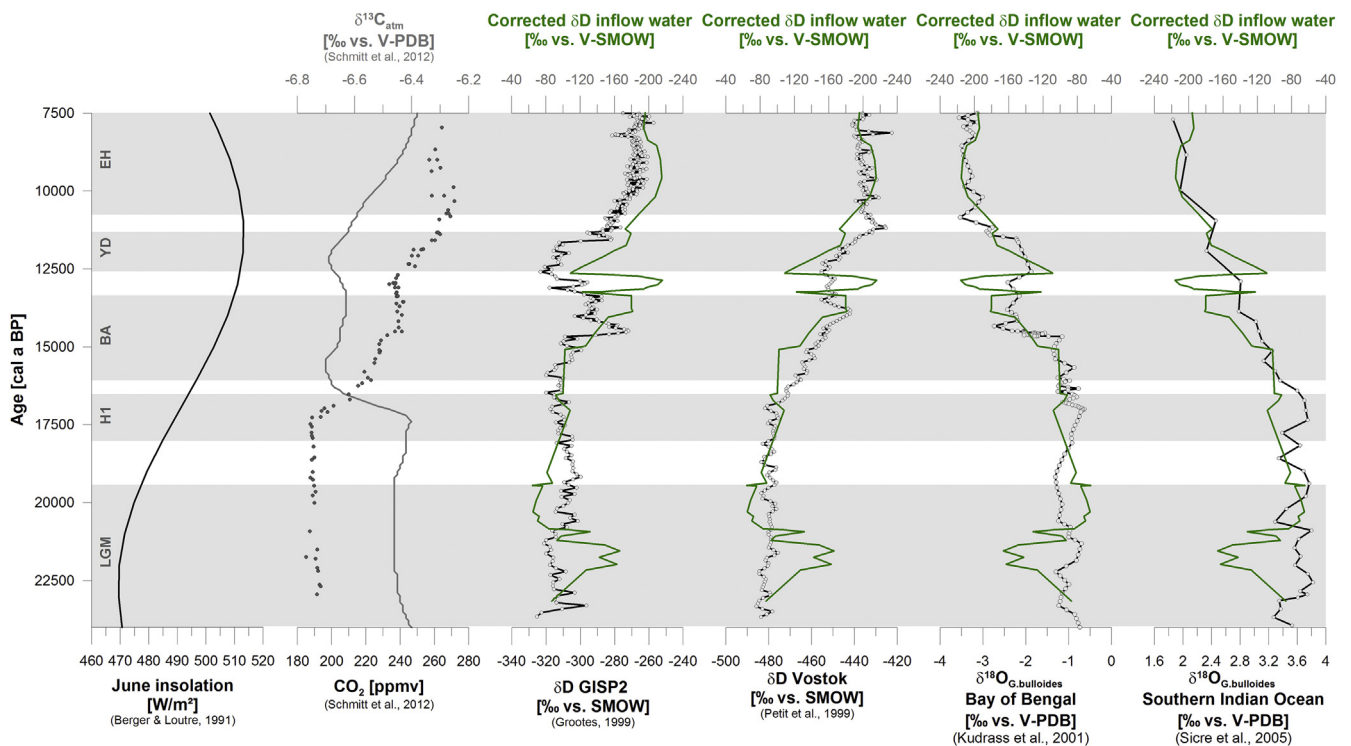


Fig. 5. Potential IOSM influencing factors (June insolation, atmospheric CO_2 and $\delta^{13}\text{C}$, δD of GISP2 and Vostok ice core, $\delta^{18}\text{O}_{\text{G. bulloides}}$ from the Bay of Bengal and the Southern Indian Ocean) in comparison with the corrected δD values of the inflow water at Nam Co. A three-point average filter was applied to the δD of inflow water to diminish the local climate signals.

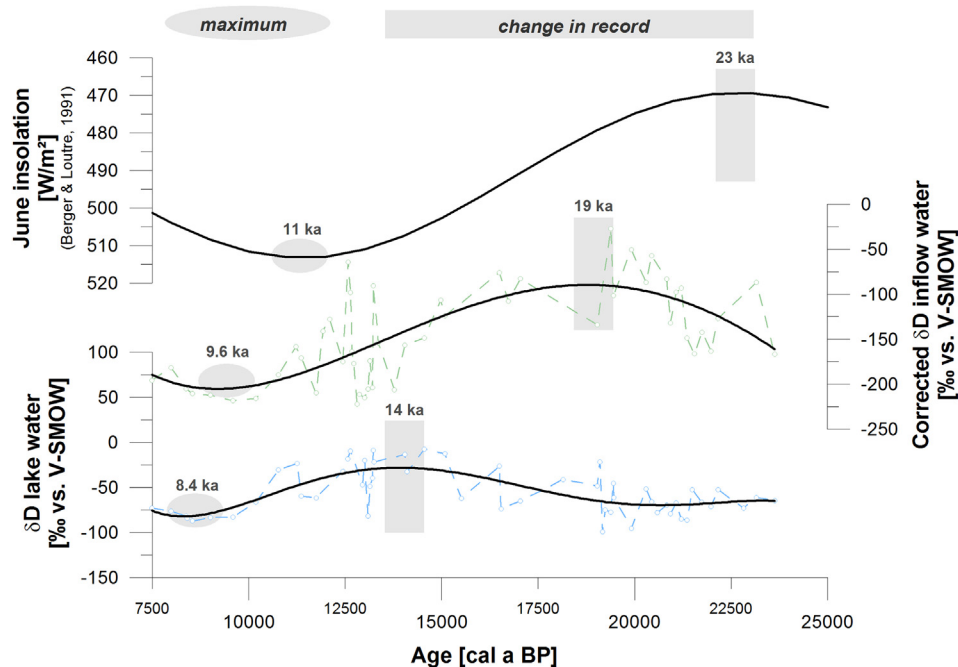


Fig. 6. Time lags between hydrogen isotope (δD) records and June insolation for time slices showing first changes (squares) and the maximum monsoon intensity (ellipses). The black lines represent the polynomial fit through the original data sets, which are plotted as dashed lines with open circles.

only by changes in the climatic system and IOSM precipitation but also by ecological factors.

After the Younger Dryas event, the aquatic system changed relatively quickly, supporting the existence of ecological thresholds in lake Nam Co. The amount of the aquatic biomarker $n\text{-C}_{23}$ increased substantially with lake surface temperatures above 4°C , pH values below 8.8 and at $\delta^{15}\text{N}$ values below 6‰ (Fig. 7). These thresholds were primarily crossed in the Holocene interglacial, which, as a result, was also characterized by a higher $n\text{-C}_{23}$

concentration (Fig. 7). Based on our data, the aquatic biological response at Nam Co depends on temperature and the associated lake size as well as ice-free seasons and nutrient availability. These ecological thresholds are crucial for the development of aquatic organisms and may explain the delayed response of the aquatic organisms compared with the terrestrial organisms.

The different reactions of aquatic ($n\text{-C}_{23}$ and their reconstructed lake water δD) and terrestrial ($n\text{-C}_{29}$ and their reconstructed inflow water δD) organisms are also obvious in the amplitude of their

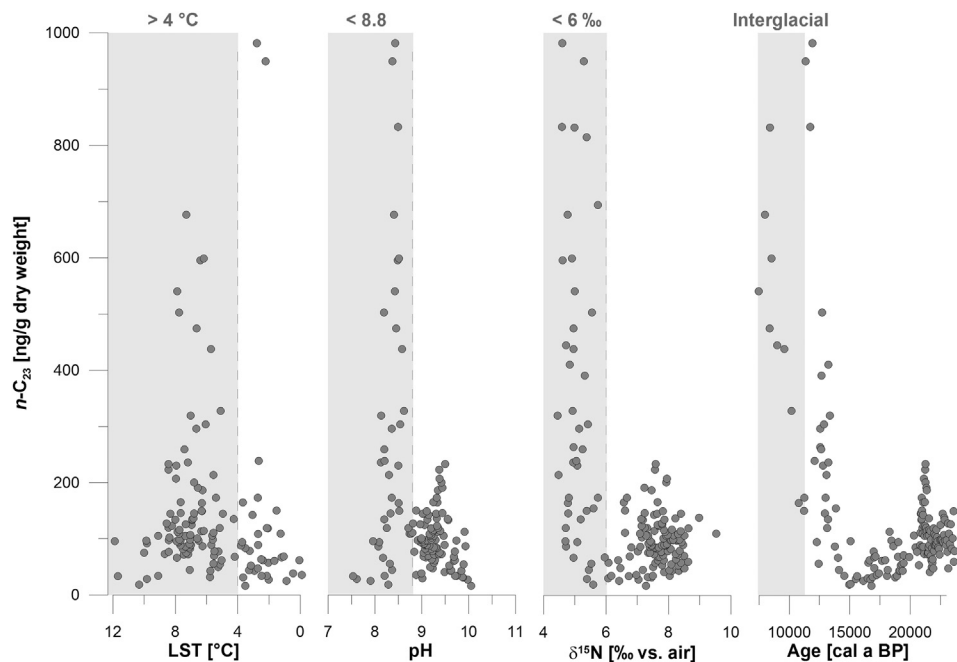


Fig. 7. Amount of aquatic n -alkane C_{23} vs. lake surface temperature (LST), pH, $\delta^{15}\text{N}$ and cal a BP showing the ecological thresholds (dashed gray line). Gray boxes indicate increased production of $n\text{-C}_{23}$.

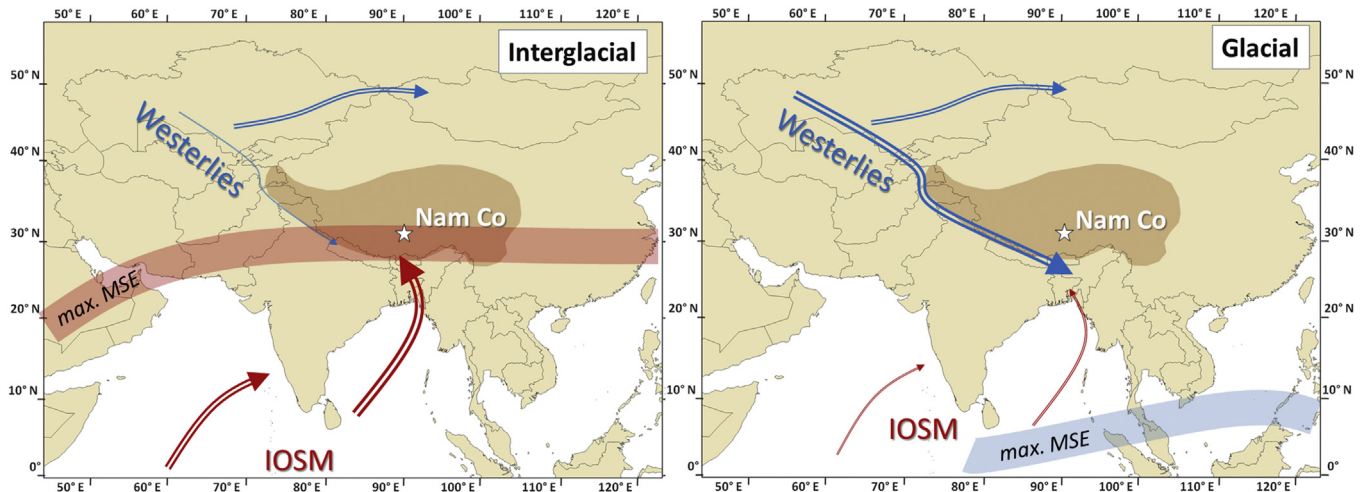


Fig. 8. Simplified summer circulation patterns displaying the influence of the Indian Ocean Summer Monsoon (IOSM) and Westerlies at Nam Co as well as the location of maximum vertically integrated moist static energy (MSE) during the Last Glacial and Holocene interglacial periods. The brown area marks the Tibetan Plateau. (For interpretation of the colors in this figure legend, the reader is referred to the web version of this article.)

isotopic records. Changes in the lake water δD only account for 91‰, while the δD values of the inflow water vary by 221‰ (Figs. 3 and 5). The terrestrial vegetation, upon which the inflow water δD values are based, mainly records a summer moisture signal modified by evapotranspiration processes. Because the terrestrial vegetation reacts more pronouncedly and more quickly to changes in the monsoonal and climatic system, the δD of $n\text{-C}_{29}$ represents an appropriate and sensitive IOSM proxy.

4.4. Potential drivers of IOSM

As discussed above, the consistent pattern in the records of δD $n\text{-C}_{29}$, $\delta^{18}\text{O}_{\text{carb}}$ and $\delta^{18}\text{O}_{G.\text{bulloides}}$ suggests that the IOSM is primarily influenced by the same driving mechanisms in the investigated study areas. In general, the IOSM can be influenced by internal and external factors. Numerous studies have already determined precession-driven insolation as one of the main external driving factors (Clemens et al., 1991; Neff et al., 2001). We compared our reconstructed δD records for the lake and inflow water with the June insolation at 30°N (Berger and Loutre, 1991) (Fig. 6). While the insolation changes to higher values at 23 cal ka BP, the isotopic composition of the inflow water changes at 19 cal ka BP and the lake water at 14 cal ka BP, indicating an intensification of the IOSM. Comparing the maximum monsoon intensity with the maximum June insolation, the time lags only account for 1.4 and 2.6 ka, respectively. Even on the annual scale, a two-month lag already exists with maximum insolation and temperature in June, but the highest precipitation occurs in August (Laskar et al., 2004; IAEA/WMO, 2012). Together with the turn-over times of the oceanic and atmospheric circulation, the time lags in the interglacial period are understandable. However, the larger time lags of 4 and 9 ka in the glacial period show that, in addition to insolation, other factors are also important. In the glacial period, ecological factors seem to be more important for the establishment and response of the aquatic organisms. The delay of the biological response is related to changes in environmental parameters such as pH, LST and nutrients (Fig. 7).

However, insolation always leads in phase to the aquatic and terrestrial records, indicating its importance to monsoonal-forced changes in the lake system. We can confirm the idea that solar insolation is more important in controlling the IOSM in the Holocene than in the glacial periods (Overpeck et al., 1996). In warm

periods, the ice volume and snow cover is decreased. Under these conditions, solar insolation can lead to stronger heat the Tibetan Plateau, which results in a larger land–ocean pressure gradient, stronger winds, boosted water vapor transport from the Indian Ocean to the Plateau and enhanced monsoonal precipitation (Fig. 8). The concentration of CO_2 in the atmosphere as a greenhouse gas is important for further warming. A first remarkable increase in CO_2 released to the atmosphere, and a parallel depletion in $\delta^{13}\text{C}_{\text{atm}}$, is detected at 17.5 cal ka BP (Fig. 5; Schmitt et al., 2012), creating the preconditions for a stronger IOSM. In glacial periods, a lower pressure gradient is established between the Indian Ocean and the Tibetan Plateau, resulting in weaker monsoonal winds. In exchange, the Westerlies are amplified in periods with weak insolation and influence the Tibetan Plateau (Fig. 8).

Finally, we compared our paleohydrological δD record with the δD values of ice cores and the $\delta^{18}\text{O}$ values of *G. bulloides* to determine whether the atmospheric or oceanic circulation is more important for the IOSM's development (Fig. 5). All records show a good agreement, implying that the IOSM is connected to the ocean as well as to the atmospheric system, which, in addition to the solar insolation, can influence the monsoon system. As interhemispheric circulation, the IOSM is more strongly affected by the southern atmospheric circulation ($R^2 = -0.71$, $p < 0.0001$) than by the northern atmospheric circulation ($R^2 = -0.48$, $p < 0.0001$). The influence of the northern ($R^2 = 0.69$, $p < 0.0001$) and southern ($R^2 = 0.70$, $p < 0.0001$) oceanic circulation is comparable. Our results show that the IOSM dynamics are controlled by changes in solar insolation as well as the oceanic–atmospheric circulation. These coupled atmosphere–ocean interactions with the IOSM system cause links to the North Atlantic Oscillation and the El Niño–Southern Oscillation (e.g., Gupta et al., 2003; Morrill et al., 2003; Kumar et al., 2006).

5. Conclusions

We present a sedimentary record that spans the Last Glacial Maximum to the Early Holocene and extends our previously published Nam Co data covering the Holocene (Mügler et al., 2010). Our temperature and precipitation records based on lipid biomarkers allow a clear differentiation between the Last Glacial and Holocene interglacial stages. In the Holocene, the paleohydrological δD proxies show a significant agreement with distinctive IOSM

records, showing that they are recording the IOSM signals. In the Glacial, Westerlies are more dominant and affect the δD values. In our record, IOSM dynamics are embedded in the coupled atmospheric–oceanic circulations. However, the main influencing factor remains the solar insolation that drives the different global circulation systems and controls the IOSM winds by building up the pressure gradient between the Tibetan Plateau and the Indian Ocean. Other internal influencing factors, such as lake environmental parameters, must also be considered. The different response times of the aquatic and terrestrial vegetation, for example, play an important role in the IOSM reconstructions. For the first time, we present evidence of ecological thresholds that control the aquatic biological response during the Glacial–Interglacial transition. Consequently, monsoon-induced signals in lacustrine sediments strongly depend on external forcings, such as insolation, as well as internal feedback mechanisms. Our results may provide a better understanding of the driving forces of the IOSM system at the Tibetan Plateau.

Acknowledgments

This project was a joint cooperation with the Institute of Tibetan Plateau Research. We thank Wang Junbo for his support in the core retrieval. We are grateful to A. Mets, J. Ossebaer and E. Hopmans for advice and assistance in the laboratory. We also thank the International Max Planck Research School for Global Biogeochemical Cycles (IMPRS-gBGC) for scientific support. Funding of the project GL262/15 was provided by the German Research Foundation (Deutsche Forschungsgemeinschaft, DFG). We thank the MPG and CAS for additional project funding within the framework of the CAS-MPG cooperation. Presented datasets are available within the PANGAEA database.

Appendix A. Supplementary data

Supplementary data related to this article can be found at <http://dx.doi.org/10.1016/j.quascirev.2015.01.023>.

References

- An, Z., Kutzbach, J.E., Prell, W.L., Porter, S.C., 2001. Evolution of Asian monsoons and phased uplift of the Himalaya–Tibetan plateau since Late Miocene times. *Nature* 411, 62–66.
- An, Z., Colman, S.M., Zhou, W., Li, X., Brown, E.T., Jull, A.J.T., Cai, Y., Huang, Y., Lu, X., Chang, H., Song, Y., Sun, Y., Xu, H., Liu, W., Jin, Z., Liu, X., Cheng, P., Liu, Y., Ai, L., Li, X., Liu, X., Yan, L., Shi, Z., Wang, X., Wu, F., Qiang, X., Dong, J., Lu, F., Xu, X., 2012. Interplay between the Westerlies and Asian monsoon recorded in Lake Qinghai sediments since 32 ka. *Sci. Rep.* 2, 619. <http://dx.doi.org/10.1038/srep00619>.
- Berger, A., Loutre, M.F., 1991. Insolation values for the climate of the last 10 million years. *Quat. Sci. Rev.* 10, 297–317.
- Berkehammer, M., Sinha, A., Stott, L., Cheng, H., Pausata, F.S.R., Yoshimura, K., 2012. An abrupt shift in the Indian Monsoon 4000 years ago. *Geophys. Monogr. Ser.* 198, 75–78.
- Bintanja, R., van de Wal, R.S.W., Oerlemans, J., 2005. Modelled atmospheric temperatures and global sea levels over the past million years. *Nature* 437, 125–128.
- Blaga, C.I., Reichert, G.J., Schouten, S., Lotter, A.F., Werne, J.P., Kosten, S., Mazzeo, N., Lacerot, G., Sinninghe Damsté, J.S., 2010. Branched glycerol dialkyl glycerol tetraethers in lake sediments: can they be used as temperature and pH proxies? *Org. Geochem.* 41, 1225–1234.
- Clark, I.D., Fritz, P., 1997. *Environmental Isotopes in Hydrogeology*. CRC Press, Boca Raton, FL, p. 328.
- Clemens, S., Prell, W., Murray, D., Shimmield, G., Weedon, G., 1991. Forcing mechanisms of the Indian Ocean monsoon. *Nature* 353, 720–725.
- Daut, G., Mäusbacher, R., Baade, J., Gleixner, G., Kroemer, E., Mügler, I., Wallner, J., Wang, J., Zhu, L., 2010. Late Quaternary hydrological changes inferred from lake level fluctuations of Nam Co (Tibetan Plateau, China). *Quat. Int.* 218, 86–93.
- Doberschütz, S., Frenzel, P., Haberzettl, T., Kasper, T., Wang, J., Zhu, L., Daut, G., Schwalb, A., Mäusbacher, R., 2013. Monsoonal forcing of Holocene paleoenvironmental change on the central Tibetan Plateau inferred using a sediment record from Lake Nam Co (Xizang, China). *J. Paleolimnol.* 51, 253–266.
- Feng, Z.-D., An, C.B., Wang, H.B., 2006. Holocene climatic and environmental changes in the arid and semi-arid areas of China: a review. *Holocene* 16, 119–130.
- Fry, B., 1991. Stable isotope diagrams of freshwater food webs. *Ecology* 71, 2293–2297.
- Geyh, M.A., Schotterer, U., Grosjean, M., 1998. Temporal changes of the ^{14}C reservoir effect in lakes. *Radiocarbon* 40, 921–931.
- Groote, P., Stuiver, M., 1999. GISP2 Oxygen Isotope Data. <http://dx.doi.org/10.1594/PANGAEA.56094>.
- Grubbs, F.E., 1969. Procedures for detecting outlying observations in samples. *Technometrics* 11, 1–21.
- Günther, F., Aichner, B., Yao, T., Gleixner, G., 2013. A synthesis of hydrogen isotope variability and their hydrological significance at the Qinghai–Tibetan Plateau. *Quat. Int.* 313–314, 3–16. <http://dx.doi.org/10.1016/j.quaint.2013.07.013>.
- Günther, F., Thiele, A., Gleixner, G., Xu, B., Yao, T., Schouten, S., 2014. Distribution of bacterial and archaeal ether lipids in soils and surface sediments of Tibetan lakes: implications for GDGT-based proxies in saline lakes. *Org. Geochem.* 67, 19–30.
- Gupta, A.K., Anderson, D.M., Overpeck, J.T., 2003. Abrupt changes in the Asian southwest monsoon during the Holocene and their links to the North Atlantic Ocean. *Nature* 421, 354–357.
- Hayes, J.M., 1993. ^{13}C contents of sedimentary organic compounds: principles and evidence. *Mar. Geol.* 113, 111–125.
- Herzschuh, U., 2006. Palaeo-moisture evolution in monsoonal Central Asia during the last 50,000 years. *Quat. Sci. Rev.* 25, 163–178.
- Hren, M.T., Bookhagen, B., Blisniuk, P.M., Booth, A.L., Chamberlain, C.P., 2009. $\delta^{18}O$ and δD of streamwaters across the Himalaya and Tibetan Plateau: Implications for moisture sources and paleoelevation reconstructions. *Earth Planet. Sci. Lett.* 288, 20–32.
- Huggett, A.J., 2005. The concept and utility of ‘ecological thresholds’ in biodiversity conservation. *Biol. Conserv.* 124, 301–310.
- Huguot, C., Hopmans, E.C., Febo-Ayala, W., Thompson, D.H., Sinninghe Damsté, J.S., Schouten, S., 2006. An improved method to determine the absolute abundance of glycerol dibiphytanyl glycerol tetraether lipids. *Org. Geochem.* 37, 1036–1041.
- IAEA/WMO, 2012. Global Network of Isotopes in Precipitation. The GNIP Database. Accessible at: <http://www.iaea.org/water>.
- Ji, J.F., Shen, J., Balsam, W., Chen, J., Liu, L.W., Liu, X.Q., 2005. Asian monsoon oscillations in the northeastern Qinghai–Tibet Plateau since the late glacial as interpreted from visible reflectance of Qinghai Lake sediments. *Earth Planet. Sci. Lett.* 233, 61–70.
- Ju, L., Wang, H., Jiang, D., 2007. Simulation of the Last Glacial Maximum climate over East Asia with a regional climate model nested in a general circulation model. *Palaeogeogr. Palaeoclimatol. Palaeoecol.* 248, 376–390.
- Kasper, T., Haberzettl, T., Doberschütz, S., Daut, G., Wang, J., Zhu, L., Nowaczyk, N., Mäusbacher, R., 2012. Indian Ocean Summer Monsoon (IOSM)-dynamics within the past 4 ka recorded in the sediments of Lake Nam Co, central Tibetan Plateau (China). *Quat. Sci. Rev.* 39, 1–13.
- Kasper, T., Haberzettl, T., Wang, J., Daut, G., Doberschütz, S., Zhu, L., Mäusbacher, R., 2015. Hydrological variations on the Central Tibetan Plateau since the LGM and their teleconnection to inter-regional and hemispheric climatic variations. *J. Quat. Sci.* 30, 70–78. <http://dx.doi.org/10.1002/jqs.2759>.
- Keil, A., Berking, J., Mügler, I., Schütt, B., Schwalb, A., Steeb, P., 2010. Hydrological and geomorphological basin and catchment characteristics of Lake Nam Co, South-Central Tibet. *Quat. Int.* 218, 118–130.
- Kendall, C., 1998. Tracing nitrogen sources and cycling in catchments. In: Kendall, C., McDonnell, J.J. (Eds.), *Isotope Tracers in Catchment Hydrology*. Elsevier, Amsterdam, pp. 519–576.
- Kudrass, H.R., Hofmann, A., Dose, H., Emeis, K., Erlenkeuser, H., 2001. Modulation and amplification of climatic changes in the Northern Hemisphere by the Indian summer monsoon during the past 80 ky. *Geology* 29, 63–66.
- Kumar, K.K., Rajagopalan, B., Hoerling, M., Bates, G., Cane, M., 2006. Unraveling the Mystery of Indian Monsoon failure during El Niño. *Science* 314, 115–119.
- Laskar, J., Robutel, P., Joutel, F., Gastineau, M., Correia, A.C.M., Lévêque, B., 2004. A long term numerical solution for the insolation quantities of the Earth. *Astron. Astrophys.* 428, 261–285.
- Laws, E., Popp, B., Bidigare, R.R., Kennicutt, M., Macko, S.A., 1995. Dependence of phytoplankton carbon isotopic composition on growth rate and $[CO_2]_{aq}$: theoretical considerations and experimental results. *Geochim. Cosmochim. Acta* 59, 1131–1138.
- Leber, D., Holawe, F., Häusler, H., 1995. Climatic classification of the Tibet Autonomous Region using multivariate statistical methods. *Geojournal* 37, 451–473.
- Li, C., Kang, S., Zhang, Q., Kaspari, S., 2007. Major ionic composition of precipitation in the Nam Co region, Central Tibetan Plateau. *Atmos. Res.* 85, 351–360.
- Li, C., Yanai, M., 1996. The onset and interannual variability of the Asian summer monsoon in relation to land–sea-contrast. *J. Clim.* 9, 358–375.
- Liu, X.Q., Shen, J., Wang, S.M., Wang, Y.B., Liu, W.G., 2007. Southwest monsoon changes indicated by oxygen isotope of ostracode shells from sediments in Qinghai Lake since the late Glacial. *Chin. Sci. Bull.* 52, 539–544.
- Meyers, P.A., 1994. Preservation of elemental and isotopic source identification of sedimentary organic matter. *Chem. Geol.* 114, 289–302.
- Meyers, P.A., Ishiwatari, R., 1995. Organic matter accumulation records in lake sediments. In: Lerman, A., Imboden, D., Gat, J. (Eds.), *Physics and Chemistry of Lakes*. Springer, Berlin, pp. 279–328.
- Morrill, C., Overpeck, J.T., Cole, J.E., 2003. A synthesis of abrupt changes in the Asian summer monsoon since the last deglaciation. *Holocene* 13, 465–476.

- Morrill, C., Overpeck, J.T., Cole, J.E., Liu, K., Shen, C., Tang, L., 2006. Holocene variations in the Asian monsoon inferred from the geochemistry of lake sediments in central Tibet. *Quat. Res.* 65, 232–243.
- Mügler, I., Sachse, D., Werner, M., Xu, B., Wu, G., Yao, T., Gleixner, G., 2008. Effect of lake evaporation on δD values of lacustrine *n*-alkanes: a comparison of Nam Co (Tibetan Plateau) and Holzmaar (Germany). *Org. Geochem.* 39, 711–729.
- Mügler, I., Gleixner, G., Günther, F., Mäusbacher, R., Daut, G., Schütt, B., Berking, J., Schwalb, A., Schwark, L., Xu, B., Yao, T., Zhu, L., Yi, C., 2010. A multi-proxy approach to reconstruct hydrological changes and Holocene climate development of Nam Co, Central Tibet. *J. Paleolimnol.* 43, 625–648.
- Neff, U., Burns, S.J., Mangini, A., Mudelsee, M., Fleitmann, D., Matter, A., 2001. Strong coherence between solar variability and the monsoon in Oman between 9 and 6 kyr ago. *Nature* 411, 290–293.
- Overpeck, J., Anderson, D., Trumbore, S., Prell, W., 1996. The southwest Indian Monsoon over the last 18000 years. *Clim. Dyn.* 12, 213–225.
- Pedentchouk, N., Freeman, K.H., Harris, N.B., 2006. Different response of δD values of *n*-alkanes, isoprenoids, and kerogen during thermal maturation. *Geochim. Cosmochim. Acta* 70, 2063–2072.
- Peterse, F., van der Meer, J., Schouten, S., Weijers, J.W.H., Fierer, N., Jackson, R.B., Kim, J.H., Sinninghe Damsté, J.S., 2012. Revised calibration of the MBT-CBT paleotemperature proxy based on branched tetraether membrane lipids in surface soils. *Geochim. Cosmochim. Acta* 96, 215–229.
- Petit, J.R., Jouzel, J., Raynaud, D., Barkov, N.I., Barnola, J.M., Basile, I., Bender, M., Chappellaz, J., Davis, J., Delaygue, G., Delmotte, M., Kotlyakov, V.M., Legrand, M., Lipenkov, V., Lorius, C., Pépin, L., Ritz, C., Saltzman, E., Stievenard, M., 1999. Climate and atmospheric history of the past 420,000 years from the Vostok Ice Core, Antarctica. *Nature* 399, 429–436.
- Polissar, P.J., Freeman, K.H., Rowley, D.B., McInerney, F.A., Currie, B.S., 2009. Paleothermometry of the Tibetan Plateau from *D/H* ratios of lipid biomarkers. *Earth Planet. Sci. Lett.* 287, 64–76.
- Rothe, J., Gleixner, G., 2004. Application of stable nitrogen isotopes to investigate food-web development in regenerating ecosystems. In: Temperton, V.M., Hobbs, R.J., Nuttle, T., Halle, S. (Eds.), *Assembly Rules and Restoration Ecology: Bridging the Gap between Theory and Practice*. Island Press, Washington, pp. 245–264.
- Sachse, D., Radke, J., Gleixner, G., 2006. δD values of individual *n*-alkanes from terrestrial plants along a climatic gradient – implications for the sedimentary biomarker record. *Org. Geochem.* 37, 469–483.
- Sachse, D., Billault, I., Bowen, G.J., Chikaraishi, Y., Dawson, T.E., Feakins, S.J., Freeman, K.H., Magill, C.R., McInerney, F.A., van der Meer, M.T.J., Polissar, P., Robins, R.J., Sachs, A.L., Schmidt, H.-L., Sessions, A.L., White, J.W.C., West, J.B., Kahmen, A., 2012. Molecular paleohydrology: interpreting the hydrogen-isotopic composition of lipid biomarkers from photosynthesizing organisms. *Annu. Rev. Earth Planet. Sci.* 40, 221–249.
- Schimmelmann, A., Lewan, M.D., Wintsch, R.P., 1999. *D/H* isotope ratios of kerogen, bitumen, oil, and water in hydrous pyrolysis of source rocks containing kerogen types I, II, IIS, and III. *Geochim. Cosmochim. Acta* 63, 3751–3766.
- Schmitt, J., Schneider, R., Elsig, J., Leuenberger, D., Laurantou, A., Chappellaz, J., Köhler, P., Joos, F., Stocker, T.F., Leuenberger, M., Fischer, H., 2012. Carbon isotope constraints on the deglacial CO_2 rise from ice cores. *Science* 336, 711–714.
- Schoon, P.L., de Kluijver, A., Middelburg, J.J., Downing, J.A., Sinninghe Damsté, J.S., Schouten, S., 2013. Influence of lake water pH and alkalinity on the distribution of core and intact polar branched glycerol dialkyl glycerol tetraethers (GDGTs) in lakes. *Org. Geochem.* 60, 72–82.
- Schouten, S., Hopmans, E.C., Schefuß, E., Sinninghe Damsté, J.S., 2002. Distributional variations in marine crenarchaeotal membrane lipids: a new organic proxy for reconstructing ancient sea water temperatures? *Earth Planet. Sci. Lett.* 204, 265–274.
- Schouten, S., Hopmans, E.C., Sinninghe Damsté, J.S., 2013. The organic geochemistry of glycerol dialkyl glycerol tetraether lipids: a review. *Org. Geochem.* 54, 19–61.
- Schouten, S., Hugué, C., Hopmans, E.C., Kienhuis, M.V.M., Sinninghe Damsté, J.S., 2007. Analytical methodology for TEX₈₆ paleothermometry by high-performance liquid chromatography/atmospheric pressure chemical ionization-mass spectrometry. *Anal. Chem.* 79, 2940–2944.
- Schrag, D.P., Hampt, G., Murray, D.W., 1996. Pore fluid constraints on the temperature and oxygen isotopic composition of the glacial ocean. *Science* 272, 1930–1932.
- Sessions, A.L., Burgoyne, T.W., Schimmelmann, A., Hayes, J.M., 1999. Fractionation of hydrogen isotopes in lipid biosynthesis. *Org. Geochem.* 30, 1193–1200.
- Shakun, J.D., Burns, S.J., Fleitmann, D., Kramers, J., Matter, A., Al-Subary, A., 2007. A high-resolution, absolute-dated deglacial speleothem record of Indian Ocean climate from Socotra Island, Yemen. *Earth Planet. Sci. Lett.* 259, 442–456.
- Sicre, M.-A., Labeyrie, L.D., Ezat, U., Duprat, K., Turon, J.L., Schmidt, S., Michel, E., Mazaud, A., 2005. Mid-latitude Southern Indian Ocean response to Northern Hemisphere Heinrich events. *Earth Planet. Sci. Lett.* 240, 724–731.
- Sinha, A., Cannariato, K.G., Stott, L.D., Li, H.C., You, C.F., Cheng, H., Edwards, R.L., Singh, I.B., 2005. Variability of Southwest Indian summer monsoon precipitation during the Bølling-Allerød. *Geology* 33, 813–816.
- Sinninghe Damsté, J.S., Ossebaer, J., Abbas, B., Schouten, S., Verschuren, D., 2009. Fluxes and distribution of tetraether lipids in an equatorial African lake: constraints on the application of the TEX₈₆ paleothermometer and branched tetraether lipids in lacustrine settings. *Geochim. Cosmochim. Acta* 73, 4232–4249.
- Steinbeiss, S., Temperton, V.M., Gleixner, G., 2008. Mechanisms of short-term soil carbon storage in experimental grasslands. *Soil Biol. Biochem.* 40, 2634–2642.
- Tian, L., Masson-Delmotte, V., Stievenard, M., Yao, T., Jouzel, J., 2001. Tibetan Plateau summer monsoon northward extent revealed by measurements of water stable isotopes. *J. Geophys. Res.* 106 (D22), 28081–28088.
- Thompson, L.G., Yao, T., Davis, M.E., Henderson, K.A., Mosley-Thompson, E., Lin, P.N., Beer, J., Synal, H.A., Cole-Dai, J., Bolzan, J.F., 1997. Tropical climate instability: the last glacial cycle from a Qinghai-Tibetan ice core. *Science* 276, 1821–1825.
- Wang, J., Zhu, L., Daut, G., Ju, J., Lin, X., Wang, Y., Zhen, X., 2009. Investigation of bathymetry and water quality of Lake Nam Co, the largest lake on the central Tibetan Plateau, China. *Limnology* 10, 149–158.
- Wang, H., Liu, W., Zhang, C.L., Wang, Z., Wang, J., Liu, Z., Dong, H., 2012. Distribution of glycerol dialkyl glycerol tetraethers in surface sediments of Lake Qinghai and surrounding soil. *Org. Geochem.* 47, 78–87.
- Wang, R.L., Scarpitta, S.C., Zhang, S.C., Zheng, M.P., 2002. Later Pleistocene/Holocene climate conditions of Qinghai-Xizhang Plateau (Tibet) based on carbon and oxygen stable isotopes of Zabuye Lake sediments. *Earth Planet. Sci. Lett.* 203, 461–477.
- Wang, P., Clemens, S., Beaufort, L., Braconnot, P., Ganssen, G., Jian, Z., Kershaw, P., Sarnthein, M., 2005. Evolution and variability of the Asian monsoon system: state of the art and outstanding issues. *Quat. Sci. Rev.* 24, 595–629.
- Wang, Y.V., Larsen, T., Leduc, G., Andersen, N., Blanz, T., Schneider, R.R., 2013. What does leaf wax δD from a mixed C_3/C_4 vegetation region tell us? *Geochim. Cosmochim. Acta* 111, 128–139.
- Weijers, J.W.H., Schouten, S., van den Donker, J.C., Hopmans, E.C., Sinninghe Damsté, J.S., 2007. Environmental controls on bacterial tetraether membrane lipid distribution in soils. *Geochim. Cosmochim. Acta* 71, 703–713.
- Werner, R.A., Bruch, B.A., Brand, W.A., 1999. ConFlo III – an interface for high precision $\delta^{13}C$ and $\delta^{15}N$ analysis with an extended dynamic range. *Rapid Commun. Mass Spectrom.* 13, 1237–1241.
- Werner, R.A., Brand, W.A., 2001. Referencing strategies and techniques in stable isotope ratio analysis. *Rapid Commun. Mass Spectrom.* 15, 501–519.
- Wu, G., Liu, Y., He, B., Bao, Q., Duan, A., Jin, F.F., 2012. Thermal controls on the Asian summer monsoon. *Sci. Rep.* 2, 1–7.
- Wünnemann, B., Damske, D., Tarasov, P., Kotlia, B.S., Reinhardt, C., Bloemendal, J., Diekmann, B., Hartmann, K., Krois, J., Riedel, F., Arya, N., 2010. Hydrological evolution during the last 15 kyr in the Tso Kar lake basin (Ladakh, India), derived from geomorphological, sedimentological and palynological records. *Quat. Sci. Rev.* 29, 1138–1155.
- Yan, D., Wünnemann, B., 2014. Late Quaternary water depth changes in Hala Lake, northeastern Tibetan Plateau, derived from ostracod assemblages and sediment properties in multiple sediment records. *Quat. Sci. Rev.* 95, 95–114.
- Zheng, M.P., Liu, J.Y., Ma, Z.B., Wang, H.L., Ma, N.N., 2011. Carbon and oxygen stable isotope values and microfossils at 41.4–4.5 ka BP in Tai Co, Tibet, China, and their paleoclimatic significance. *Acta Geol. Sin. (English Edition)* 85, 1036–1056.
- Zhu, D., Meng, X., 2004. On the Quaternary Environmental Evolution of the Nam Co Area, Tibet. *Geology Press, Beijing*, pp. 1–93 (in Chinese with English abstract).